Dielectric Properties of Intergrowth Ferroelectrics in the System $Bi_{2.5}Na_{m-1.5}Nb_mO_{3m+3}$ (m= 2, 3 &4).

A THESIS SUBMITTED IN PARTIAL FULFILLMENT OF

THE REQUIREMENTS FOR THE DEGREE OF

BACHELOR OF TECHNOLOGY

By

PUSHPENDRA SINGH

Roll no: - 109CR0679

DEPARTMENT OF CERAMIC ENGINEERING
NATIONAL INSTITUTE OF TECHNOLOGY
ROURKELA
2012-2013

Dielectric Properties of Intergrowth Ferroelectrics in the System $Bi_{2.5}Na_{m-1.5}Nb_mO_{3m+3}$ (m= 2, 3 & 4)

A THESIS SUBMITTED IN PARTIAL FULFILLMENT OF

THE REQUIREMENTS FOR THE DEGREE OF

BACHELOR OF TECHNOLOGY

By

PUSHPENDRA SINGH

Roll No: - 109CR0679

UNDER THE GUIDANCE OF

DR. JAPES BERA

DEPARTMENT OF CERAMIC ENGINEERING
NATIONAL INSTITUTE OF TECHNOLOGY
ROURKELA
2012-2013

NATIONAL INSTITUTE OF TECHNOLOGY
ROURKELA

CERTIFICATE

This is to certify that the thesis entitled, “Dielectric Properties of Intergrowth Ferroelectrics in the System $Bi_{2.5}Na_{m-1.5}Nb_mO_{3m+3}$ (m= 2, 3 & 4),” submitted by Pushpendra Singh in partial fulfilment of the requirements of the award of Bachelor of Technology Degree in Ceramic Engineering at National Institute Of Technology, Rourkela is an authentic work carried out by him under my supervision and guidance.

To the best of my knowledge, the matter embodied in the thesis has not been submitted to any other university / institute for the award of any Degree or Diploma.

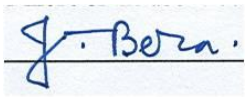

Date:

Dr. Japes Bera
(Associate Professor)
Dept. of Ceramic Engineering
National Institute of Technology
Rourkela-769008

Acknowledgement

I wish to express my deep sense of respect and regard for Prof. Japes Bera, Department of Ceramic Engineering, N.I.T Rourkela for introducing the research topic and for his inspiring guidance, constructive criticism and valuable suggestions throughout this research work. I would also like to thank him for his constant support and words of encouragement without which it would not have been possible for me to complete this research work.

I am also grateful to all the faculty members of the Dept. of Ceramic Engineering, whose immense knowledge in the field of ceramics has enlightened me in various areas of my research work.

I am also grateful to Mr Ganesh Kumar Sahoo, Miss Geetanjali Parida and all the other research scholars in the Dept. of Ceramic Engineering for their unparalleled help and support.

I am also thankful to Mr Prashant Mohanty, Mr Sushil Sahoo and all the other office staff for all their help. I would also like to thank my friends for all their suggestions and inputs for the betterment of my research work.

Finally, I deeply thank my parents for all their support and faith in me.

PUSHPENDRA SINGH
Roll No:- 109CR0679
B.Tech, Dept. of Ceramic Engineering
N.I.T Rourkela

Date:

ABSTRACT

The Aurivillius phases are bismuth layer structure ferroelectric compounds [BLSF]. These compounds received increase interest due to their properties which are suitable for varieties of technical devices like ferroelectric memories, high temperature piezoelectric, catalyst application etc.

In this thesis, BLSF compound in the system $Bi_{2.5}Na_{m-1.5}Nb_mO_{3m+3}$(m= 2, 3 & 4) were successfully synthesised through solid oxide reaction route, through analysing their decomposition behaviour using DSC-TG instrument. Pure phases of individual compound and their intergrowths were formed after calcination at 800^oC. The powders were sintered to more than 90% of their theoretical density. The powder and sintered ceramics were characterize for their phase formation by XRD analysis, lattice parameter determination, bulk density of sintered product by Archimedes principle, microstructural analysis using scanning electron microscope. For dielectric and ferroelectric properties measurement, silver electrodes were applied in the specimen and the properties were measure using LCR meter in the frequency range 1 kHz -1 MHz The ferroelectric polarisation behaviour with applied electric field of these compounds was evaluated using ferroelectric loop tracer. The intergrowth compounds show higher dielectric and ferroelectric properties compare to their individual compounds. So the intergrowth compounds may be suitable for high frequency dielectric application.

Contents **page**

List of figures

List of tables

CHAPTER 1

INTRODUCTION

Introduction

Bismuth layer-structured ferroelectrics (BLSFs) were first reported by Aurivillius in 1949 [1]. BLSFs are highly promising as ferroelectric non-volatile random access memory (FRAM) storage devices, high temperature piezoelectric device applications, sensor applications, and as photo-catalyst [2-5]. They also possess some attractive electrical properties such as excellent fatigue endurance, fast switching speed, good polarization retention, relatively high Curie temperature, low aging rate and low operating voltage [6-9].

The commercially available lead based piezoelectric materials possess high piezoelectric coefficients [12]. However, lead based materials are banned due to their hazardous nature under the Environmental pollution act. Other lead free piezoelectric materials like $BaTiO_3$ possess low Curie temperature which hinders their high temperature applications. BLSFs based piezoelectric materials have Curie temperature and are strong competitor in the development of lead free high temperature piezoelectric materials.

The structure of BLSF consists of intergrowth of fluorite-like $(Bi_2O_2)^{2+}$ units and pseudo-perovskite slabs $(A_{n-1}B_nO_{3n+1})^{2-}$ as shown in Fig. 1. *A* is a relatively large size mono-, di- or tri-valent cation in 12-coordination site. This site is occupied by cations such as Na^+, K^+ , Ba^{2+}, Ca^{2+}, Sr^{2+}, Pb^{2+}, Bi^{3+}. As shown in Figure 1, Sr^{2+} and Bi^{3+} are the *A*-type cations. *B* is a small size, highly charged tetra-, penta- or hexa-valent cation in the octahedral coordination site of pseudo-perovskite unit. The site is generally occupied by Ti^{4+}, Ta^{5+}, Nb^{5+}, V^{5+}, W^{6+}. For example, Ta^{5+} is the *B*-type cations (Fig.1). $(A_{n-1}B_nO_{3n+1})^{2-}$ perovskite slabs are sandwiched between Bi_2O_2 layers giving a characteristic layer structure. *n* indicates the number of perovskite units

stacked along the *c*-axis between $(Bi_2O_2)^{2+}$ layers. It has values in the range $1 \leq n \leq 8$ [1, 13, 14]. Some typical examples of BLSFs are: Bi_2WO_6 (n = 1), $SrBi_2Nb_2O_9$ (n = 2), $Bi_4Ti_3O_{12}$ (n = 3), $PbBi_4Ti_4O_{15}$ (n = 4) and $Ba_2Bi_4Ti_5O_{18}$ (n = 5). Fig.1.1 shows a typical two layer $SrBi_2Ta_2O_9$, n = 2 [15] BLSFs.

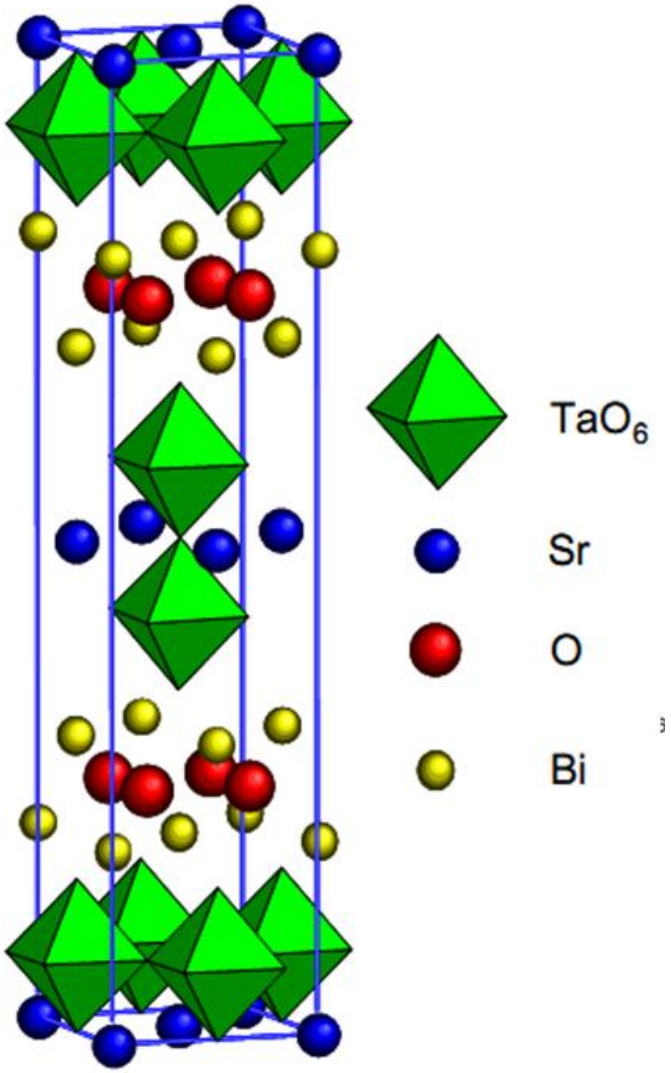

Fig.1. Typical structure of $SrBi_2Ta_2O_9$ (n = 2) BLSFs.

At room temperature, most of the BLSFs possess non-Centro-symmetric orthorhombic structure. Ferroelectricity of BLSF compounds arises because of the three main distortions in the orthorhombic structure. The distortions are: tilting of the oxygen octahedra (a) around the *a*-axis, (b) around the *c*-axis, and (c) a shift of *A*

and/or *B*-cations along the polar *a*-axis [17, 18]. Ferroelectricity mainly arises in the perovskite blocks [19]. Bi_2O_2 layers perform the function of an insulating layer and controls the electrical response such as electrical conductivity, band gap, *etc*. [20, 21].

One of the most appealing advantages of BLSF compounds is their compositional flexible nature which allows modifying their properties according to the chemical composition. The members show various properties depending on the type of the cations occupying the *A* and *B*-site of BLSF. Also the donor substitution improves the resistivity of the BLSF which generally have oxygen vacancies due to bismuth volatilization during high temperature processing. Acceptor and donor co-substitution at *A* and/or *B*-site of BLSFs have been found very effective to change the relaxor behaviour by forming localized charged polar pairs.

Present thesis is related to these compounds in the system $Bi_{2.5}Na_{m-1.5}Nb_mO_{3m+3}$ with m= 2, 3, and 4.The BLSF compounds are $Bi_{2.5}Na_{0.5}Nb_20_9$ (m=2), $Bi_{2.5}Na_{1.5}Nb_30_{12}$ (m=3) and $Bi_{2.5}Na_{2.5}Nb_40_{15}$ (m=4). There are very few reports on this system. The structure of $Bi_{2.5}Na_{1.5}Nb_30_{12}$ (NBN-3) and $Bi_{2.5}Na_{2.5}Nb_40_{15}$ (NBN-4) have been reported by Kikuchi [22]. After that, $Bi_{2.5}Na_{0.5}Nb_20_9$ (NBN-2) along with NBN-3 and NBN-4 were reported by Stefan Borg et al [23] as shown in Fig. 2.

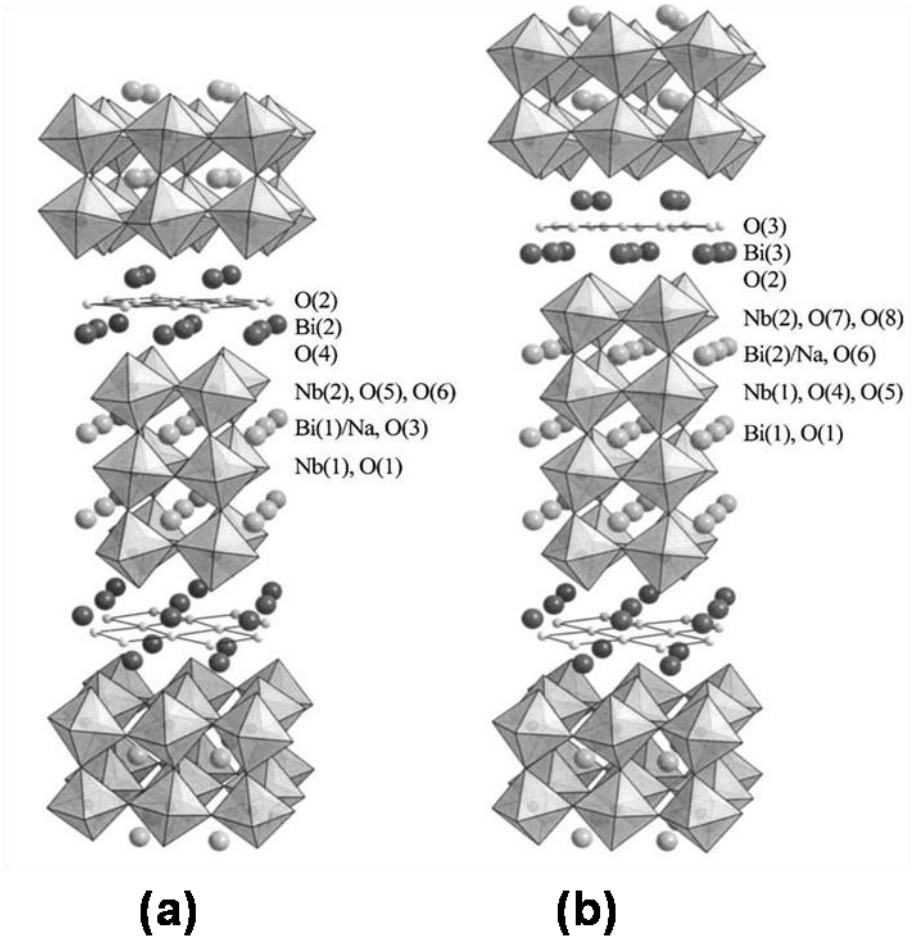

Fig. 2 Perspective drawings of (a) $Bi_{2.5}Na_{1.5}Nb_30_{12}$, and (b) $Bi_{2.5}Na_{2.5}Nb_40_{15}$ [23].

At 1977, the intergrowth of the BLSF was discovered by Kikuchi et. al. [24, 25], which have better ferroelectric properties than their individuals. The general formula of this kind of intergrowth compound can be written as: $Bi_4A_{m+n-2}B_{m+n}O_{3(m+n)+6}$,. m and n are number of BO_6 octahedral layers in the perovskite layer interleaved with $(Bi_2O_2)^{2+}$ sheets where sum of m and n are odd number. For example, $SrBi_8Ti_7O_{27}$ intergrowth, a structure built up by an intergrowth of half unit cell of $Bi_4Ti_3O_{12}$ and a half of unit cell of $SrBi_4Ti_4O_{15}$ structure in the direction of their common c-axis [25]. $Bi_4Ti_3O_{12}$-$BaBi_4Ti_4O_{15}$ (BIT-BBT), Bi4Ti3O12-$SrBi_4Ti_4O_{15}$ are some intergrowth materials which have good electrical and piezoelectric properties than the individuals

[26 - 29]. The spontaneous polarization of BIT-BBT single crystal is 52μC/cm^2 which is larger than those of individuals BIT and BBT crystals. Due to the relatively large remnant polarization, $Bi_4Ti_3O_{12}$-$SrBi_4Ti_4O_{15}$ is the promising intergrowth materials as compared to the other intergrowth [26,30, 31].

However, there are no reports available about the dielectric and ferroelectric properties of these compounds or their intergrowths.

Objectives

1) First objective is the in-situ synthesis of $Bi_{2.5}Na_{0.5}Nb_20_9$- $Bi_{2.5}Na_{1.5}Nb_30_{12}$ & $Bi_{2.5}Na_{0.5}Nb_20_9$- $Bi_{2.5}Na_{2.5}Nb_40_{15}$intergrowths ferroelectrics.

2) Second objective is to evaluate the change in dielectric and ferroelectric properties of above two intergrowth ceramics compare to the individual ferroelectrics.

CHAPTER 2

EXPERIMENTAL

Introduction

$Bi_{2.5}Na_{0.5}Nb_20_9$, $Bi_{2.5}Na_{1.5}Nb_30_{12}$, $Bi_{2.5}Na_{2.5}Nb_40_{15}$, $Bi_{2.5}Na_{0.5}Nb_20_9$-$Bi_{2.5}Na_{1.5}Nb_30_{12}$ & $Bi_{2.5}Na_{1.5}Nb_30_{12}$- $Bi_{2.5}Na_{2.5}Nb_40_{15}$ is synthesized in the present investigation, are listed in Table 3.1. The compositions will be abbreviated as NBN-2, NBN-3, NBN-4 and NBN2-3 & NBN3-4 respectively.

All these ceramics were synthesized through solid oxide route. The conventional solid state route uses simple processing steps and relatively less costly raw materials. However, the temperature requirement for the formation of pure phase powder and its densification is quite high. On the other hand, preparation of powder through the chemical method results in a more expensive. Detailed procedure is described below.

Table-1 List of compositions synthesized.

1.	Pure compound	$Bi_{2.5}Na_{0.5}Nb_20_9$
2.	Pure compound	$Bi_{2.5}Na_{1.5}Nb_30_{12}$
3.	Pure compound	$Bi_{2.5}Na_{2.5}Nb_40_{15}$
4.	Intergrowth compound	$Bi_{2.5}Na_{0.5}Nb_20_9$-$Bi_{2.5}Na_{1.5}Nb_30_{12}$
5.	Intergrowth compound	$Bi_{2.5}Na_{1.5}Nb_30_{12}$- $Bi_{2.5}Na_{2.5}Nb_40_{15}$

Synthesis of $Bi_{2.5}Na_{0.5}Nb_2O_9$

NBN-2 powder was prepared by solid state synthesis of stoichiometric quantities of bismuth oxide Bi_2O_3, sodium carbonate Na_2CO_3 and niobium pentoxide Nb_2O_5 as raw materials. All the reagents used were analytically pure. Fig. 3 shows a flow chart for the synthesis of the powders by solid oxide route.

To prepare a 5 gm. batch of NBN-2 powder, 3.33 gm. of bismuth oxide, 0.151 gm. of sodium carbonate and 1.528 gm. of niobium pentoxide was weighed separately in a weighing machine. Mix all three compositions, which were thoroughly ground in isopropanol in an agate mortar for about one an half hour before firing. The powder was calcined at 800^{o}C for 7 hours which took place in covered alumina crucibles in air.

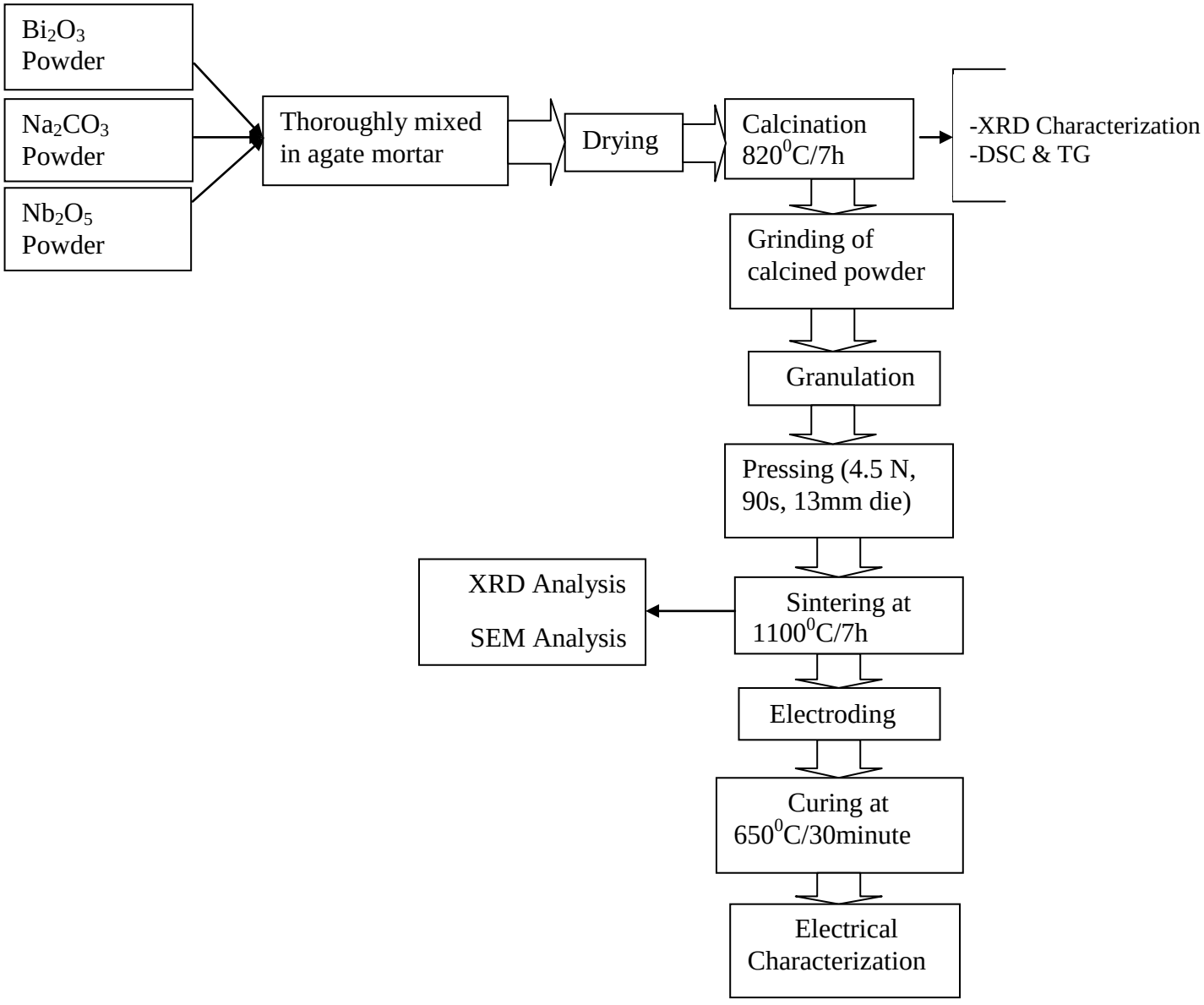

Figure 3. Generalized flow chart for synthesis of powder

Synthesis of $Bi_{2.5}Na_{1.5}Nb_30_{12}$

NBN-3 powder was prepared by solid state synthesis of stoichiometric quantities of bismuth oxide Bi_2O_3, sodium carbonate Na_2CO_3 and niobium pentoxide Nb_2O_5 as raw materials. All the reagents used were analytically pure. Fig. 3 shows a flow chart for the synthesis of the powders by solid oxide route.

To prepare a 5 gm. batch of NBN-2 powder, 2.796 gm. of bismuth oxide, 0.3815 gm. of sodium carbonate and 1.9138 gm. of niobium pentoxide was weighed separately in a weighing machine. Mix all three compositions, which were thoroughly ground in isopropanol in an agate mortar for about one an half hour before firing.

The powder was calcined at 800^oC for 7 hours which took place in covered alumina crucibles in air.

Synthesis of $Bi_{2.5}Na_{2.5}Nb_40_{15}$

NBN-4 powder was prepared by solid state synthesis of stoichiometric quantities of bismuth oxide Bi_2O_3, sodium carbonate Na_2CO_3) and niobium pentoxide Nb_2O_5as raw materials. All the reagents used were analytically pure. Fig. 3 shows a flow chart for the synthesis of the powders by solid oxide route.

To prepare a 5 gm. batch of NBN-2 powder, 2.4117 gm. of bismuth oxide, 0.5457 gm. of sodium carbonate and 2.2012 gm. of niobium pentoxide was weigh separately in a weighing machine. Mix all three compositions, which were thoroughly ground in isopropanol in an agate mortar for about one an half hour before firing. The powder was calcined at 800^oC for 7 hours which took place in covered alumina crucibles in air.

Synthesis of $Bi_{2.5}Na_{0.5}Nb_20_9$ -$Bi_{2.5}Na_{1.5}Nb_30_{12}$ Intergrowth

NBN2-3 intergrowth powder was prepared by solid state synthesis of stoichiometric quantities of bismuth oxide Bi_2O_3 , sodium carbonate Na_2CO_3 and niobium pentoxide Nb_2O_5 as raw materials. All the reagents used were analytically pure. Fig. 3 shows a flow chart for the synthesis of the powders by solid oxide route.

To prepare a 5 gm. batch of NBN-2 powder, 3.0654 gm. of bismuth oxide, 0.26795 gm. of sodium carbonate and 1.7215 gm. of niobium pentoxide was weighed separately in a weighing machine. Mix all three compositions, which were thoroughly ground in isopropanol in an agate mortar for about one an half hour before firing.

The powder was calcined at 800^{o}C for 7 hours which took place in covered alumina crucibles in air.

Synthesis of $Bi_{2.5}Na_{1.5}Nb_30_{12}$ - $Bi_{2.5}Na_{2.5}Nb_40_{15}$ Intergrowth

NBN-3-4 powder was prepared by solid state synthesis of stoichiometric quantities of bismuth oxide Bi_2O_3, sodium carbonate Na_2CO_3 and niobium pentoxide Nb_2O_5 as raw materials. All the reagents used were analytically pure. Fig. 3 shows a flow chart for the synthesis of the powders by solid oxide route.

To prepare a 5 gm. batch of NBN-2 powder, 3.0654 gm. of bismuth oxide, 0.26795 gm. of sodium carbonate and 1.7215 gm. of niobium pentoxide was weighed separately in a weighing machine. Mix all three compositions, which were thoroughly ground in isopropanol in an agate mortar for about one an half hour before firing.

The powder was calcined at 800^{o}C for 7 hours which took place in covered alumina crucibles in air.

Characterization of powder

Differential Scanning Calorimetry (DSC) and Thermo-gravimetric Analysis (TGA)

The dried precursor powder was characterized by DSC and TGA analysis using NETZSCH STA (Model No 449 C) in an ambient atmosphere with a heating rate of 10^{o}C/min. This characterization technique was used to analyse the dehydration and decomposition behaviour, the thermodynamics and phase formation behaviour of the precursor powder.

When a material is subjected to a temperature change, it absorbs or releases thermal energy due to the various physical and chemical changes undergoing in the material. DSC device evaluates the difference in temperature of the sample with respect to the reference inert material during heating or cooling. This temperature difference is measured by a differential thermocouple. Exothermic and endothermic changes are in the opposite directions of the baseline.

TGA is a simple analytical technique that measures the mass loss or mass gain of a material as a function of temperature. As materials are heated, they can lose weight due to drying or evolution of gases from chemical reactions taking place in the specimen. Some materials can gain weight by reacting with the atmospheric gases in the testing environment. The TGA plot identifies the temperature at which mass loss is maximum, corresponding to the DSC peak.

Phase analysis

X-ray diffraction is a powerful tool for material characterization. Various physical properties such as optical, ferroelectric, magnetic, electric, etc. depend on the atomic arrangement of the specimen and its chemical composition. X-ray diffraction pattern provides vital information such as: (i) qualitative phase composition of the sample, (ii) inter-planar spacing of different phases, (iii) intensities of diffraction peaks providing quantitative information of the phases, (iv) unit cell parameters and lattice type of different phases, (v) crystallite size of phases.

Phase formation of raw and calcined powder samples was studied by powder X-ray diffraction, performed with a Philip's Diffractometer (Model: PW-1830, Philips, Netherlands). The source is Cu K_α with a wavelength of 1.541874 Å and equipped with Ni β-filter. To detect the diffracted X-rays, an electronic detector is placed on the other side of the sample from the X-ray tube and the sample was rotated through different Bragg's angles.. The diffraction pattern of the sample was plotted as X-ray intensity (counts/sec) against the angle 2θ. The 2θ for each diffraction peak was converted to *d*-spacing, using the Bragg's law; $n\lambda = 2d \sin\theta$, where λ is the wave length of X-ray and n is order of diffraction.

Identification of different phases was carried out by using Philips X'pert Highscore software. The powder pattern comprises of a set of peak positions 2θ and a set of relative peak intensities *I*. But the angular position of the peaks depends on the wavelength used and a more fundamental quantity is the spacing *d* of the lattice planes forming each peak. Each pattern is described by listing the *d* and *I* values of its diffraction peaks. Each substance is characterized by *d* values of its 3 strongest peaks. *d* values together with the relative intensities are sufficient to characterize the pattern of an unknown phase.

Lattice parameters were determined in table-2 using following relationship for orthorhombic structure using the relation

$$\frac{1}{d^2} = \frac{h^2}{a^2} + \frac{k^2}{b^2} + \frac{l^2}{c^2} \qquad (1)$$

Table 2 Lattice parameter of pure NBN compound

hkl reflection	Lattice parameter		
	a	b	c
<004>			24.6424
<113>	5.43226		
<008>			24.814
<115>	5.45619		
<020>		5.4558	
<0010>			24.7979
<119>	5.51937		
<028>		5.4808	
<0012>			24.6006
<220>	5.44563		
<0210>		5.49356	
Average value	5.46336	5.47675	24.713725

where, *a*, *b* and *c* are the lattice parameters, *d* is the interplanar spacing and (*hkl*) are Miller indices and volume (*V*) of the unit cell was determined from the relation

$$V = a \times b \times c \qquad (2)$$

Fabrication of pellet and Sintering

Calcined powder of each composition was granulated with 5 wt% polyvinyl alcohol (PVA). Powder was pressed into circular disks with a 13 mm die using stearic acid as a lubricant. The powder was compacted at a load of 4.5 N with a holding time of 90 seconds. The pellets were then sintered at a temperature 1100^{o}C and in a sealed alumina crucible to minimize bismuth volatilization.

Density measurements

Densities of sintered samples were measured using Archimedes principle. The basic procedure was as follows. The dry weight of the sintered samples was measured. The sintered samples were then immersed in water and kept under a vacuum 1 hrs to ensure that water filled up the open pores completely. The suspended weight of the pellet was then measured in water. Then the soaked weight was measured by blotting the pellet with a wet towel and then weighed. The apparent porosity and bulk densities were calculated as follows:

$$\% \, \mathrm{P_{App}} = \frac{W_s - W_d}{W_s - W_a} \times 100 \qquad (3)$$

$$\mathrm{D_{bulk}} = \frac{W_d}{W_s - W_a} \qquad (4)$$

where, W_d = Dry weight of the sample , W_s = Soaked weight of the sample, W_a = Suspended weight of the sample.

Relative densities of different sintered specimens were calculated from the bulk density and theoretical density as obtained from X-ray method. As the macroscopic specimen usually does carry minute cracks and pores, its bulk density based on the sample's weight and volume is usually less than and cannot exceed the X-ray density. X-ray density is also called 'theoretical density'. However, it is not theoretical because it is determined experimentally. The base for the X-ray density for calculation is the single unit cell by defining the X-ray density equal to weight of atoms in unit cell per volume of unit cell, expressed:

$$\rho = \frac{\Sigma A_w}{NV} \qquad (5)$$

where, ρ is the X-ray density (gm/cc), ΣA_w is the sum of the atomic weights of all the atoms in the unit cell, N is the Avogadro's number and V is the volume of unit cell (cc). Orthorhombic unit cell of NBN-2, NBN-3, NBN-4, NBN-2-3 & NBN-3-4 intergrowth contains 4 formula units in one unit cell. Thus equation (5) can be written as:

$$\rho = \frac{4M_w}{N(a \times b \times c)} \qquad (6)$$

where, $M_w$is the molecular weight of one formula unit and 'a', 'b' and 'c' are the lattice parameters of the unit cell.

Microstructural study

Microstructures of the sintered specimen were studied. In SEM, a hot tungsten filament electron gun under vacuum emits electron beam which passes through a series of electromagnetic lenses. The sample is then bombarded with the fine beam of electrons having acceleration potentials ranging from 1 to 15 kV. A part of the beam is reflected as back scattered electrons (BSE) along with low energy secondary electron emission (SE).

Images formed from the BSE beam were studied in the extrinsic mode of SEM. The images appeared very real as if photographed by ordinary means. The apparent illumination is a function of particle emission rather than radiation. The emitted back scattered electrons are detected and displayed on a scanning TV display. An image will be the result of high electron emission, while the primary influence on high emission is the surface structure of the specimen. The end result is therefore brightness associated with surface characteristics and an image which looks very much like a normally illuminated object.

The micrographs of the sintered samples were recorded without any coating. Images formed from the back scattered electrons were studied by SEM, inconjunction with EDX for elemental analysis. The microstructure of the samples was different of each sample according to their composition. 4 layered compositions have more elongated grains in compare to 3 and 2 layer compositions.

Electroding and Electrical Property Measurements

Dielectric Measurements

For electrical measurements, both thesurfaces of pellets were painted uniformly with a silver conductive paste and cured at 650^{o}C for 30 minute.Thus a pellet with two parallel electrodes acts as a single layer capacitor.

The capacitance (C) of this disc capacitor and dielectric loss ($tan\delta$) of the same were measured. Data were collected in the frequency range 1 kHz – 1 MHz The instrument applies a sinusoidal voltage to the dielectric, and the magnitude and phase shift of the resultant current were measured.

When a dielectric is subjected to an electric field, a current flows. This total current flowing in a dielectric is made up of two parts: (a) conduction current and (b) displacement current. The displacement current is the elastic response of the dielectric material to the applied electric field. When the amplitude of the electric field is increased, the additional displacement gets stored within the dielectric as potential energy. As the amplitude of the electric field is decreased, the dielectric releases some amount of its stored energy as the displacement current. This displacement current can be separated into a vacuum contribution and the other part as resulting from the dielectric by the relation:

$$D = \varepsilon_o E + P \qquad (7)$$

where, *E* is the electric field and *P* is the polarization of the dielectric.

The capacitance of a dielectric capacitor arises due to dielectric polarization. Dielectric polarization may be described as the separation of bound charges in a dielectric material into positive and negative charge entities when subjected to an electric field. There are different types of polarization occurring in a material. They are electronic, ionic, dipolar and space charge polarization.. The total polarization of a material is the sum of all the four polarization.

The dielectric loss (tan δ) is the measure of energy dissipated in a dielectric on application of an electric field, which can be expressed as the ratio of resistive (loss) component of the current to the capacitive component of the current.

$$tan\,\delta = \frac{I_l}{I_c} = \frac{\varepsilon''}{\varepsilon'} \qquad (8)$$

Polarization versus Electric field study

The hysteresis loop measurement was carried out by a *P-E* loop tracer (Marine India Electronics). The instrument is based on the Sawyer-Tower method.

For these measurements, the thickness of the pellets were taken in account.The pellets were electroded with silver paint and cured at 650^{o}C for 30 minute. All the measurements were carried out at room temperature.

Materials exhibiting ferroelectricity must be solids composed of crystallites and must also possess reversible spontaneous polarization which can be reversed on the application of an external electric field. Spontaneous polarization means a nonzero polarization value in the absence of an electric field and the direction of which can be reversed by an applied field in the opposite direction. Hysteresis is one of the prominent features of ferroelectricity exhibiting a non-linear relationship between the polarization *P* and applied field *E*.

CHAPTER 3

RESULTS

and

DISCUSSION

Results and Discussion

Thermal decomposition and Phase formation behaviour

The raw precursor where Bi_2O_3, Nb_2O_5& Na_2CO_3were mixed,was used to study the thermal decomposition behaviour using differential scanning calorimetry (DSC) and thermo-gravimetric (TG).Fig.4 shows the decomposition behaviour of the precursor for NBN-2 ceramics. The decomposition reaction proceeds mainly in two steps. The initial TG weight loss (~ 1.1%) up to 100^oC corresponds to the dehydration of the precursor. Next weight loss (~ 4.2%) in the temperature range 300-1050^oC corresponds to the decarboxylation of Na_2CO_3. The endothermic peak near 100^oC is due to the dehydration of physically adsorbed water.

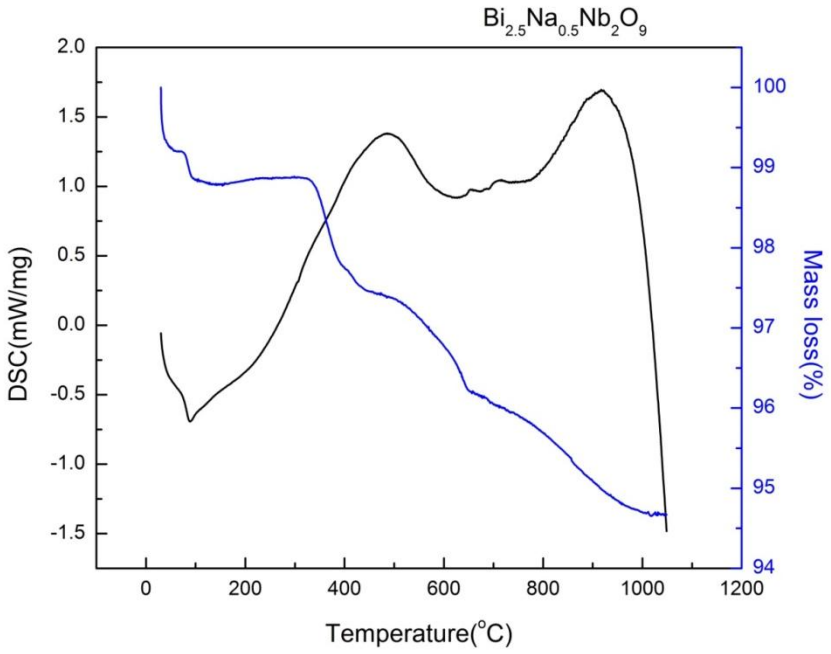

Fig.4 DSC/TG plot of precursor powder of $Bi_{2.5}\,Na_{0.5}Nb_2O_9$

The exothermic peak at about 500^oC may be due to the formation of some intermediate crystalline phases, which could be identifying only by XRD- analysis.

The second exothermic peak at 950^{o}C is due to the formation of crystalline NBN-2 BLSF compound. The formation of NBN-2 phase can be confirmed from the XRD pattern of powder that calcined at 820^{o}C and the pattern is shown in Fig.5. The pattern corresponds to pure NBN-2 phase, identified through X'Pert High Score software and matching for the compound with JCPDF No. 42-0397.

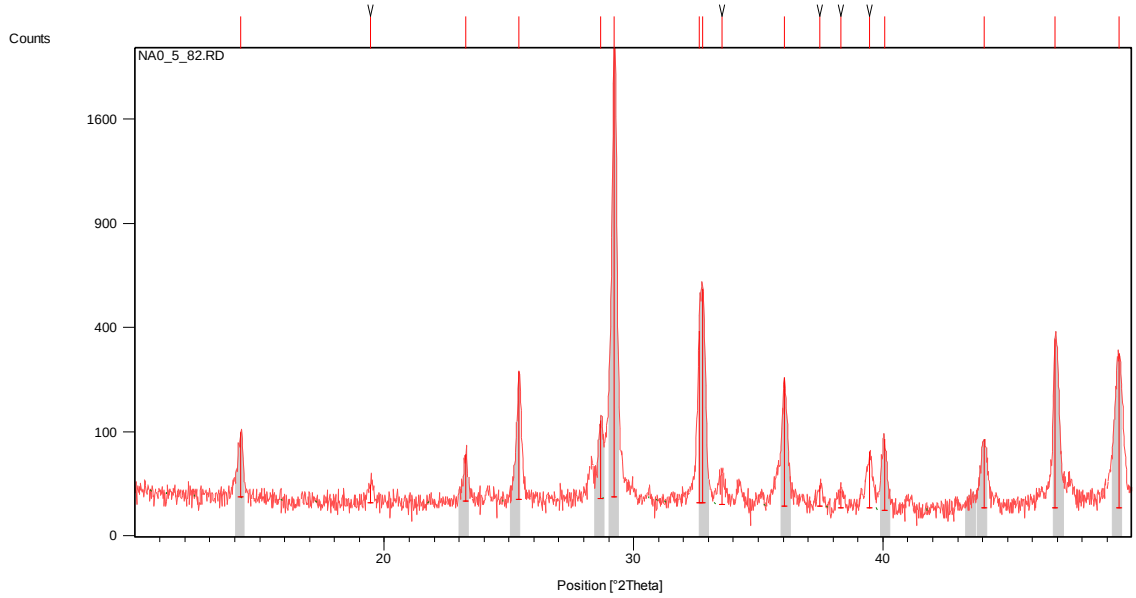

Ref. Code	Compound Name	Chemical Formula
42-0397	Sodium Bismuth Niobium Oxide	Bi2.5 Na0.5 Nb2 O9

Fig .5 XRD Analysis of calcined powder of $Bi_{2.5}Na_{0.5}Nb_2O_9$

Figure 6 shows the DSC-TG plot of the precursor powder for NBN-3 ceramics. It also shows two stages of weight losses, the first weight loss in the temperature range 100^{0}C for dehydration and the second weight loss in the temperature range 300-1000^{o}C is for decarburization of Na_2CO_3.The DSC pattern has a major exothermic peak around 950^{o}C, again due to the formation of crystalline phase NBN-3

compound. The formation of NBN-3 phase can be confirmed from the XRD pattern of powder that calcined at 820^{o}C (Fig.7). The phases in pattern of the Figure 7 were identified as NBN-2 and NBN-4. However, the formation of NBN-3 could not be identified as the X'pert Highscore software was not having the pattern of NBN-3. Since the pattern of NBN-3 is very similar to those of NBN-2 and NBN-4, it can be concluded that NBN-3 has also formed in the material.

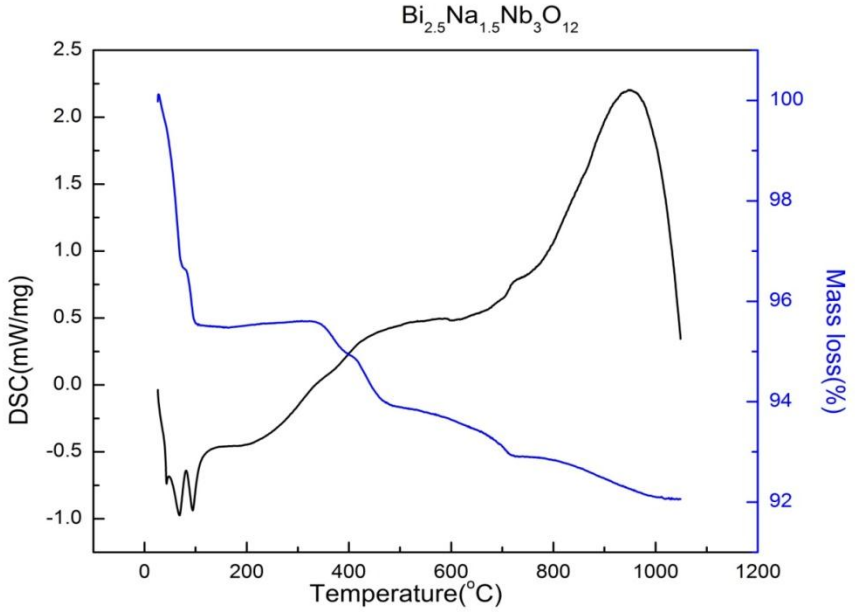

Fig.6 DSC/TG plot of precursor powder of $Bi_{2.5}Na_{1.5}Nb_3O_{12}$

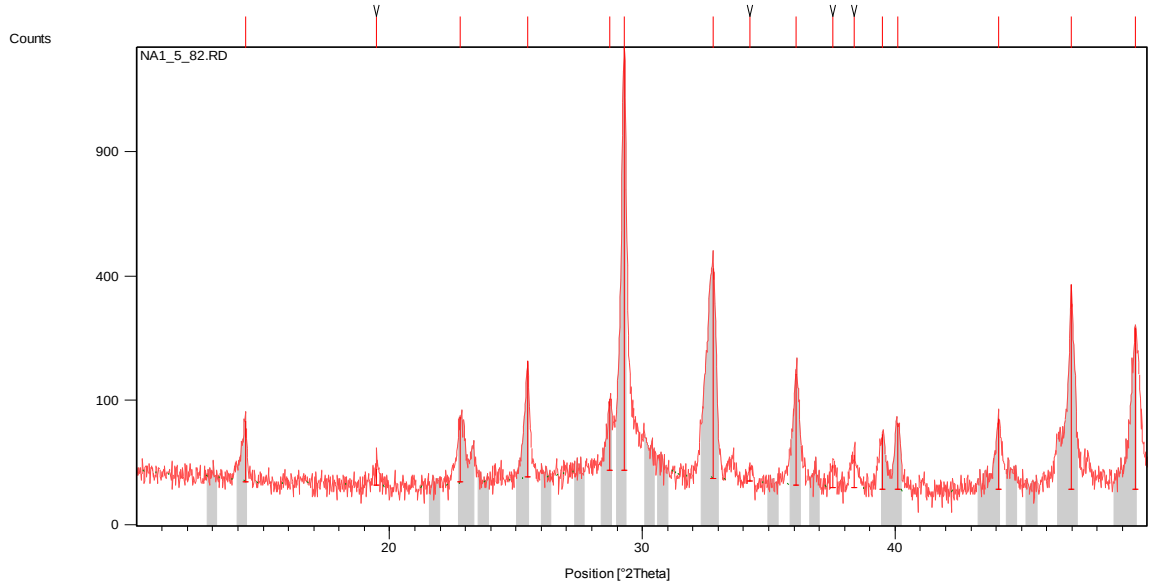

Ref. Code	Compound Name	Chemical Formula
42-0397	Sodium Bismuth Niobium Oxide	Bi2.5 Na0.5 Nb2 O9
42-0398	Sodium Bismuth Niobium Oxide	Bi2.5 Na2.5 Nb4 O15

Fig.7 XRD Analysis of calcined powder of $Bi_{2.5}Na_{1.5}Nb_3O_{12}$

Figure 8 and Figure 9 shows the DSC-TG of NBN-4 and the XRD pattern the precursor for NBN-4 after calcination at 820^{o}C. Similar results were found for the case of NBN-4. Here again the identified phases were NBN-2 and NBN-4. NBN-2 is present in the all calcined product due to the easiest formation of the 2 layer compound in BLSF system. As we know that the building block for the BLSF compound in this system is NBN-2, which converted to NBN-3 and NBN-4 respectively when the composition changes.

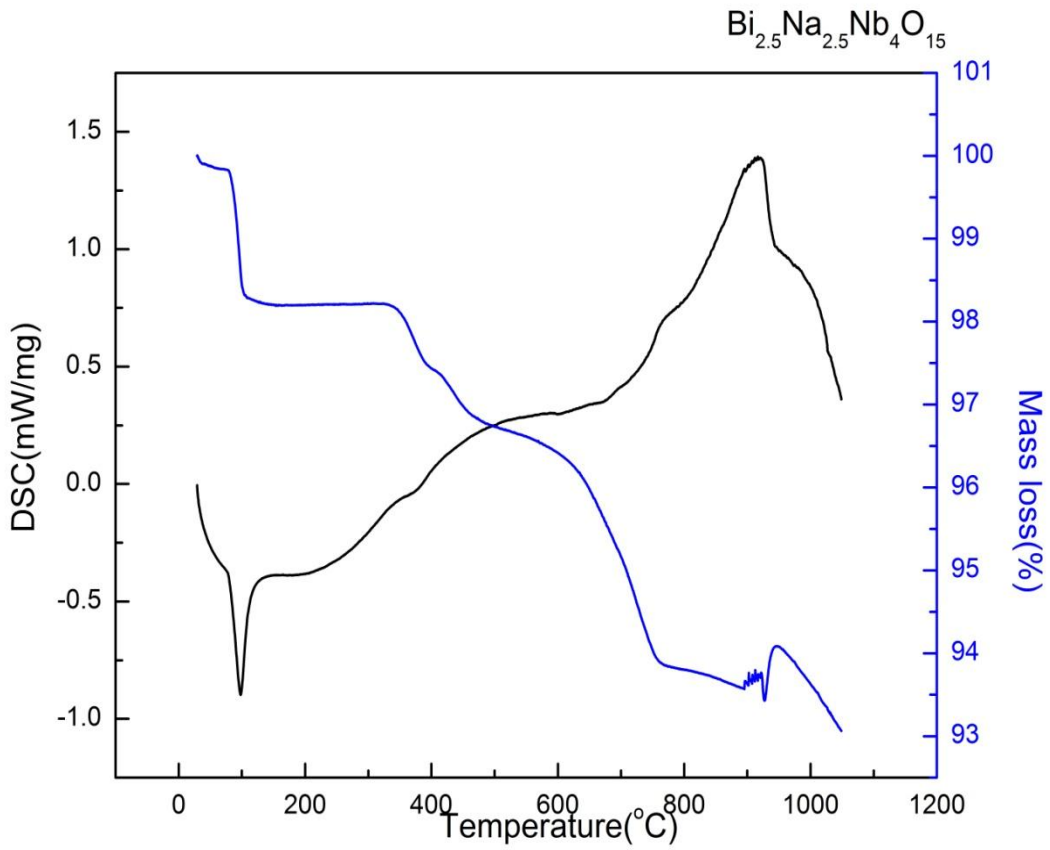

Figure 8 DSC/TG plot of precursor powder of $Bi_{2.5}Na_{2.5}Nb_4O_{15}$

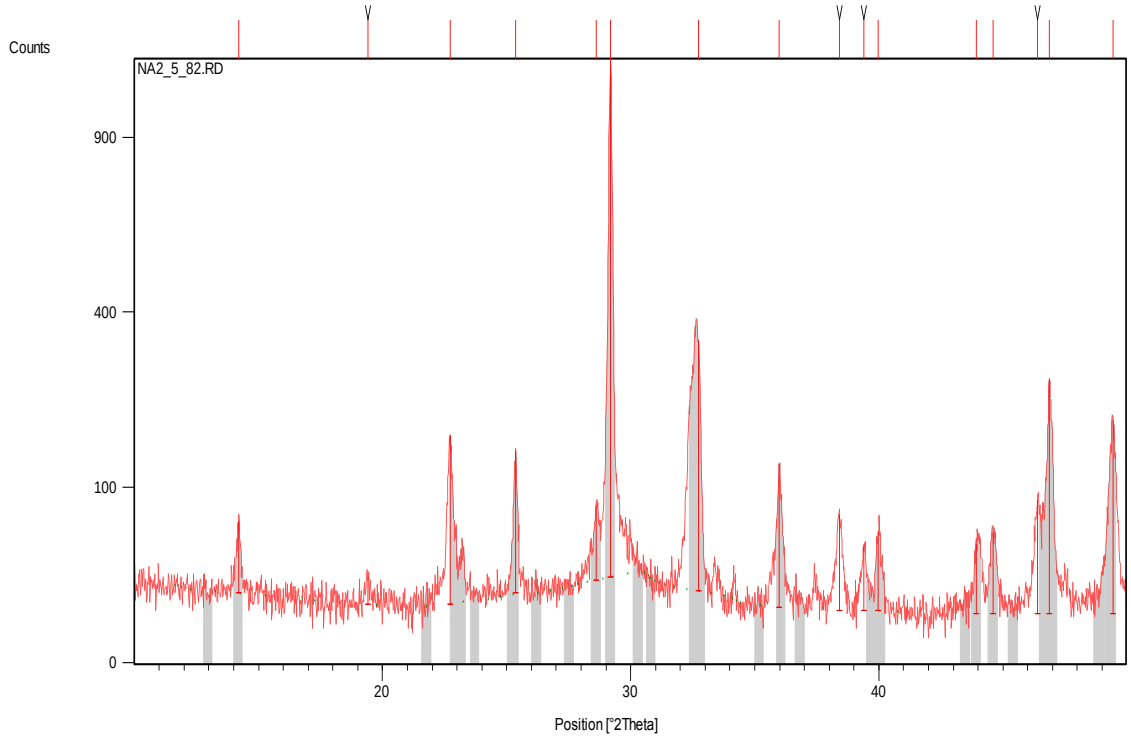

Ref. Code	Compound Name	Chemical Formula
42-0397	Sodium Bismuth Niobium Oxide	Bi2.5 Na0.5 Nb2 O9
42-0398	Sodium Bismuth Niobium Oxide	Bi2.5 Na2.5 Nb4 O15

Fig.9 XRD Analysis of calcined powder of $Bi_{2.5}Na_{2.5}Nb_4O_{15}$

NBN2-NBN3 and NBN3-NBN4 intergrowths were also synthesised by calcination at 820^{o}C. The intergrowth phases were formed in-situ during cacination of the precursor powder. Figure-10 shows the NBN2-3 intergrowth XRD pattern along with their individual NBN-2 and NBN-3 patterns. Intergrowth pattern is very similar to their individual 2 layer and 3 layer patterns. This indicates that the intergrowth was formed in the calcined product. Similar intergrowth between NBN3-NBN4 was also formed in-situ in 820^{o}C calcined powder (Fig.11).

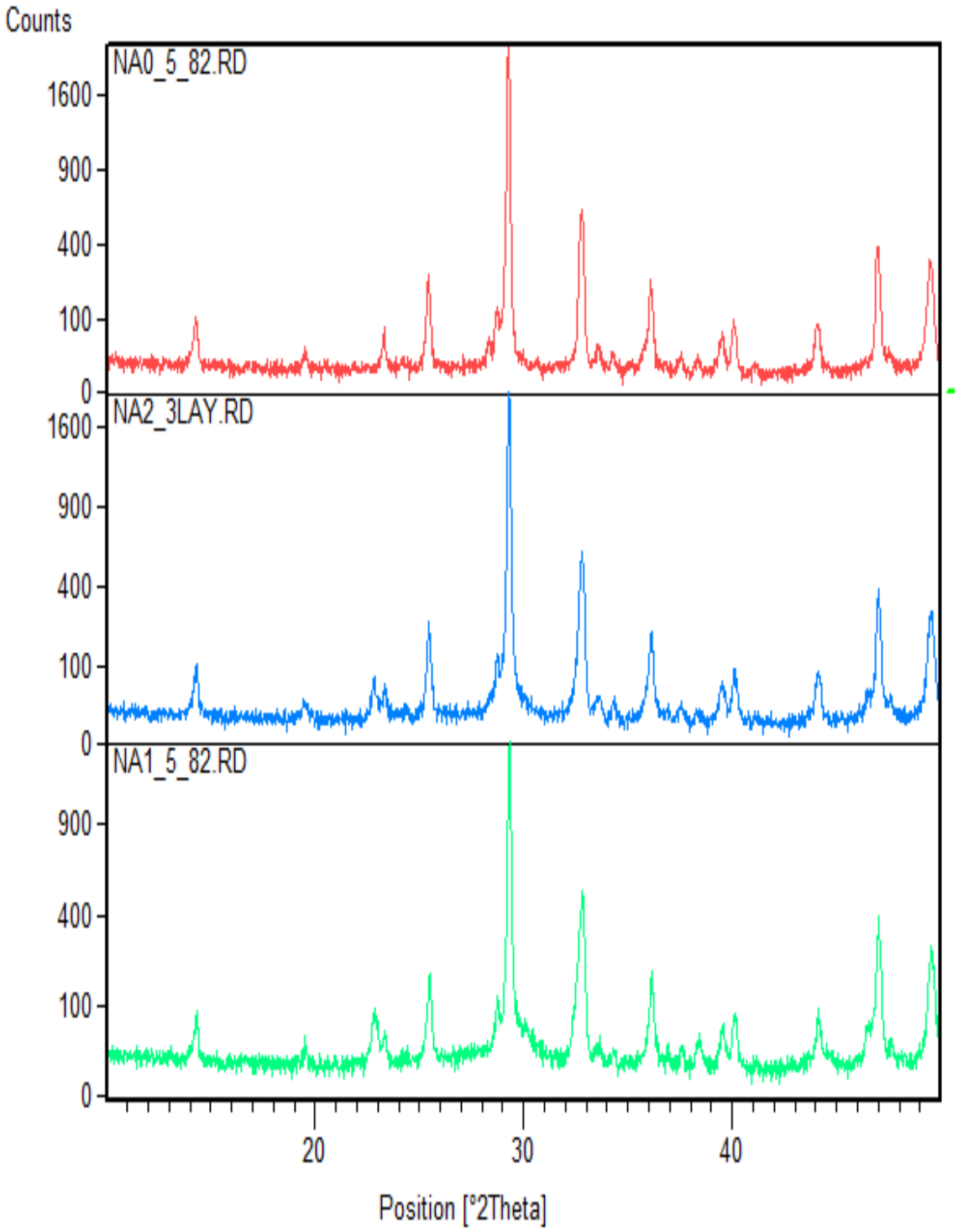

Fig. 10 XRD analysis of NBN-2-3 layer intergrowth (NA2_3 LAY) calcined powder

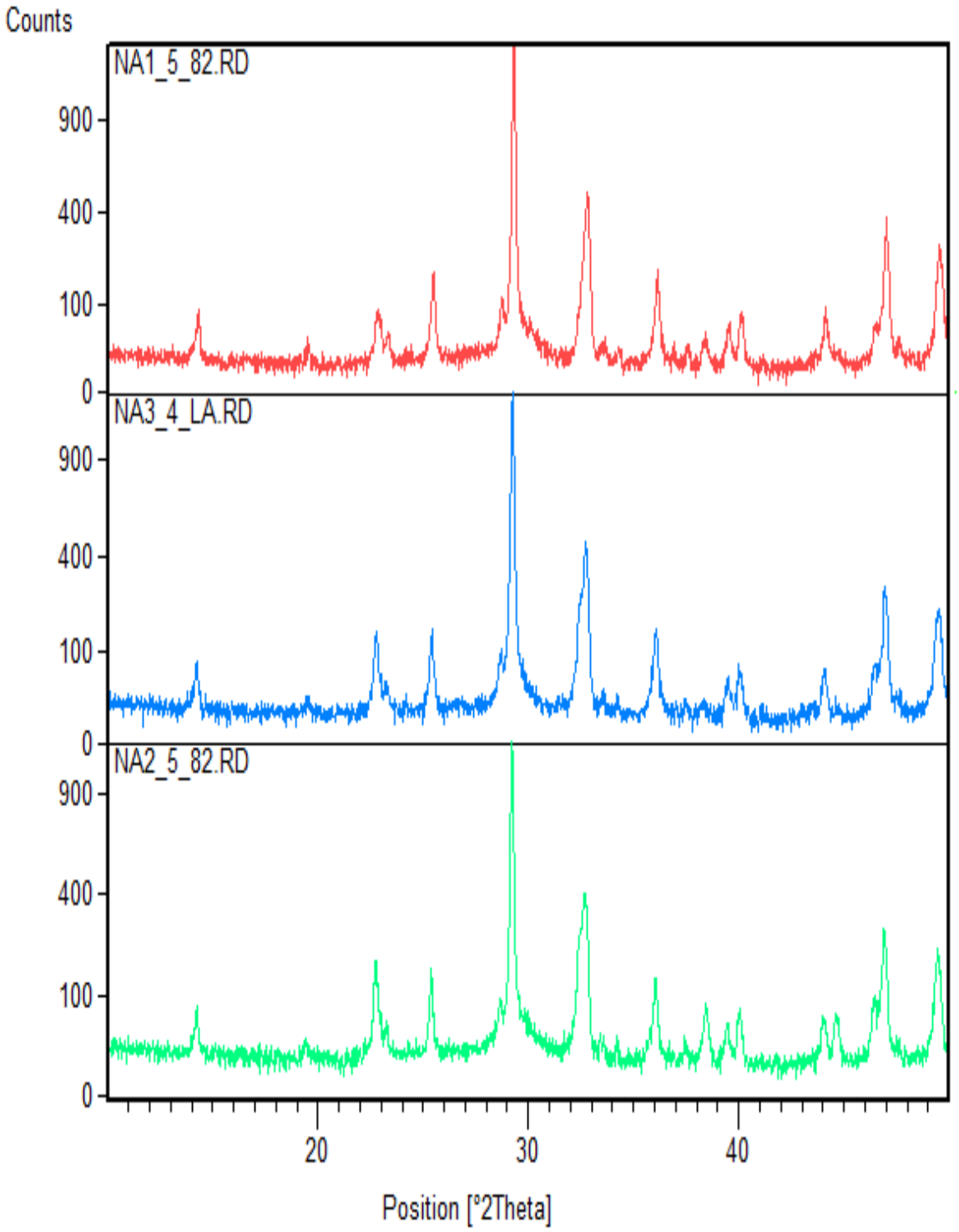

Fig.11 XRD analysis of NBN3-4 layer intergrowth (NA3_4 LA) calcined powder

Densification & sintering Behaviour

Two types of intergrowths and their individual BLSF compounds were successfully sintered at 1100^{o}C for 7 hours dwelling time. The % theoretical densities achieved for the all composition were above 90%. Their bulk density and % theoretical density are shown in Table-3. The X-ray density of each composition was calculated using their lattice parameter. The X- ray density for intergrowth compound was calculated by averaging the density of two individual BLSF compounds, considering 50:50 compositions. NBN-4 has relatively lower BD due to its very long crystal structure which required high temperature for breaking of bond and diffusion and also at that high temperature sodium, bismuth & Niobium starts volatize out of the system. That is why the BD of NBN-4 was lower and the same thing happened for 3 and 4 layer intergrowth compound due to the presence of NBN-4.

Table-3% Theoretical density of pure and their intergrowth compounds

Composition	Density and sintering temperature			
	X- ray density (g/cm^3)	Bulk density (g/cm^3)	% theoretical density	Sintering temp.
$Bi_{2.5}Na_{0.5}Nb_2O_9$	7.75	7.32	94.4	1100°C/7h
$Bi_{2.5}Na_{1.5}Nb_3O_{12}$	7.01	6.71	95.8	
$Bi_{2.5}Na_{2.5}Nb_4O_{15}$	6.55	5.91	90.25	
$Bi_{2.5}Na_{0.5}Nb_2O_9$ + $Bi_{2.5}Na_{1.5}Nb_3O_{12}$	7.35	7.11	96.78	
$Bi_{2.5}Na_{1.5}Nb_3O_{12}$ + $Bi_{2.5}Na_{2.5}Nb_4O_{15}$	6.77	6.17	91.14	

Fig.12 shows the XRD pattern of sintered pallets. The patterns were very similar to their calcined powder XRD pattern, which indicates there was no decomposition of the phases during their sintering.

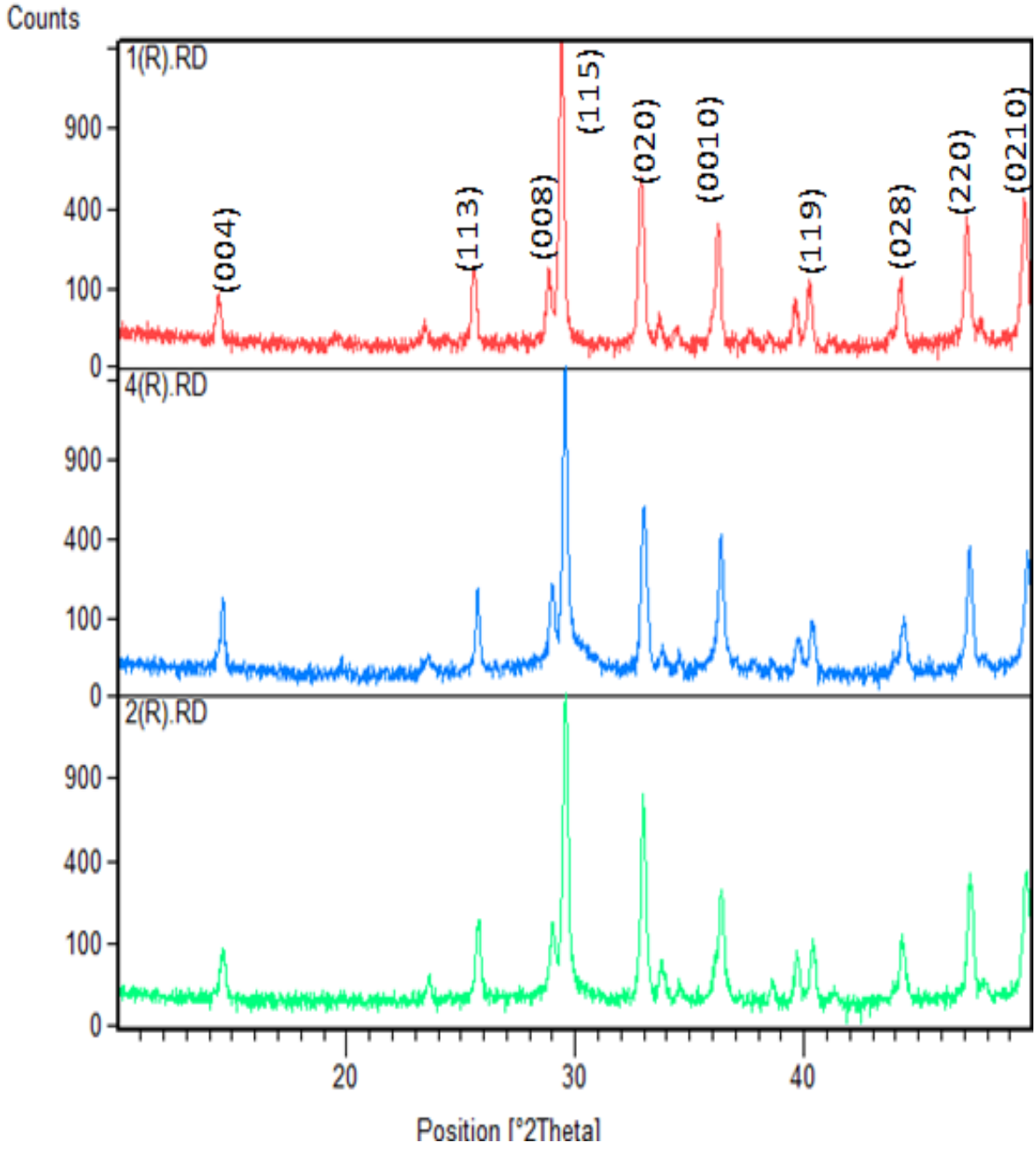

Fig. 12 XRD pattern of sintered pallets, 1(R) =NBN-2, 2(R) =NBN3 and 4(R) =NBN 2-3 intergrowth.

Microstructural Characteristics

Sintered pallets were examined for their micro-structural development using SEM. Figure-13 shows the SEM microstructure of NBN-2, NBN-3 and their intergrowths. NBN-2 microstructure Fig.13(a) shows plate like elongated grains of a NBN-2. The grains have length in the range 15-20µ and thickness in the range 5-10µ. On the other hand NBN-3 has much longer grains in the range of 30-40µ and thickness in the range of 2-5µ. This is mainly due to the lattice parameter of NBN-3 is much bigger than NBN-2, so growth of grains along a, b plane will be easy rather than along c direction. That is why length of grain in NBN-3 is much longer than their width or thickness. NBN2-NBN3 intergrowth shows simple mixer of two microstructures.

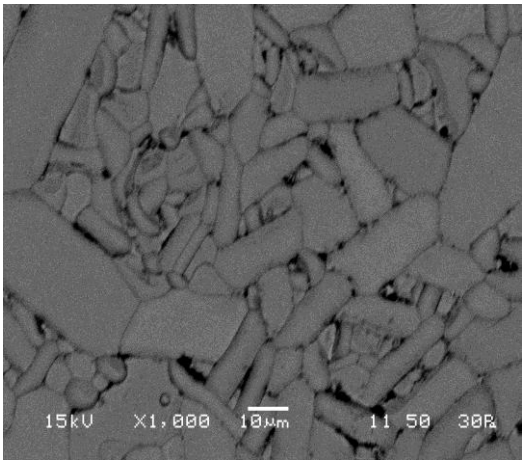

(a) $Bi_{2.5}Na_{0.5}Nb_2O_9$

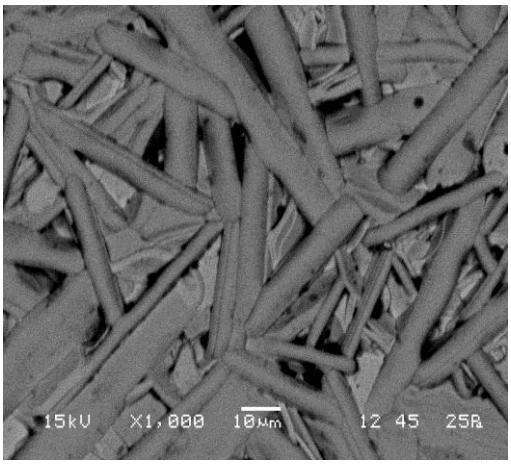

(b) $Bi_{2.5}Na_{1.5}Nb_3O_{12}$

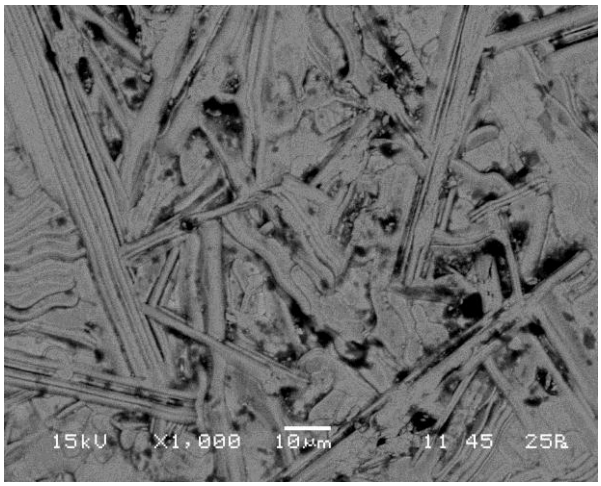

(C) $Bi_{2.5}Na_{0.5}Nb_2O_9$ - $Bi_{2.5}Na_{1.5}Nb_3O_{12}$ Intergrowth

Fig.-13SEM images of the 2, 3 & 2-3 layered compounds samples

Similarly, fig-14 shows the SEM microstructure of NBN-4 and NBN3-4 intergrowth as expected NBN-4 has very long plate compare to their thickness.

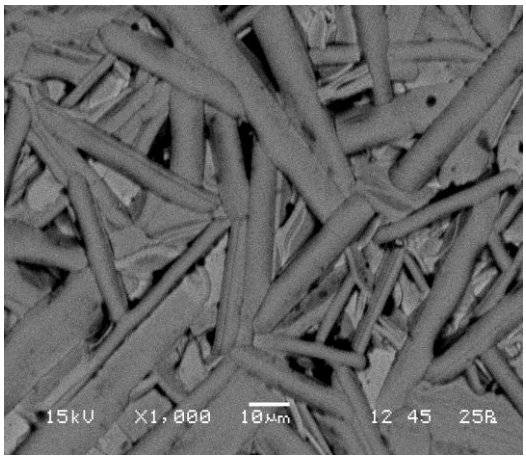

(a)$Bi_{2.5}Na_{1.5}Nb_3O_{12}$

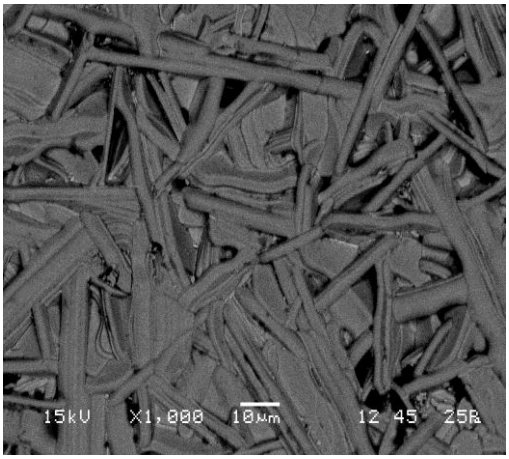

(b) $Bi_{2.5}Na_{2.5}Nb_4O_{15}$

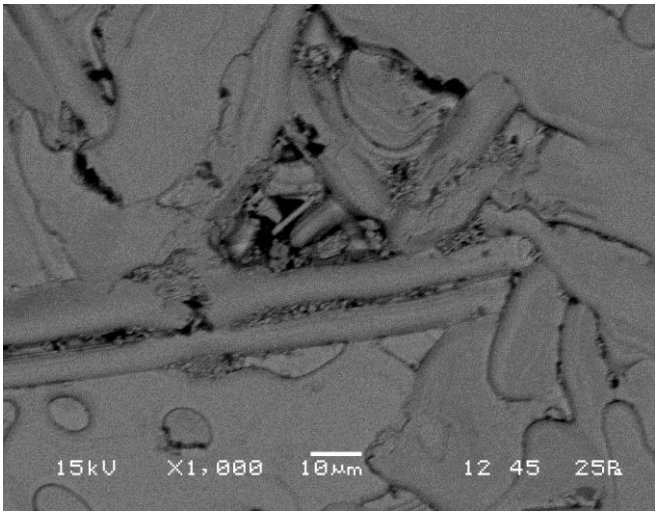

(c) $Bi_{2.5}Na_{1.5}Nb_3O_{12}$-$Bi_{2.5}Na_{2.5}Nb_4O_{15}$ Intergrowth

Fig.-14 SEM microstructure of the 3, 4 & 3-4 layered compounds samples

ELECTRICAL CHRACTERIZATION

Figure-15 shows the frequency dependency of permittivity of five different BLSF compound. The permittivity of NBN-4(NBN15) compound is higher than NBN-3(NBN12) and NBN-2(NBN9) layer compound. This is due to the presence of higher no. of perovskite layer in NBN-4. Polarisation mainly arises from perovskite layer in these compounds. It is interesting to note that NBN-3-NBN-4 intergrowth shows the highest permittivity among all due to the formation of intergrowth structure mainly. These intergrowth formation usually exert lattice strain due to the mismatch two different lattice structure which helps in increasing the polarisation in the system, however NBN-2-NBN-3 intergrowth shows lowest permittivity among all. The reason is not clear and will be investigated in future. All the permittivities are stable in the frequency range 1 kHz-1 MHz, indicating they are applicable in a wide frequency range. However their *tanδ* (Fig-16) is stable up to about 300 kHz after that it increases due to some resonance loss phenomena which will also be investigated in detailed.

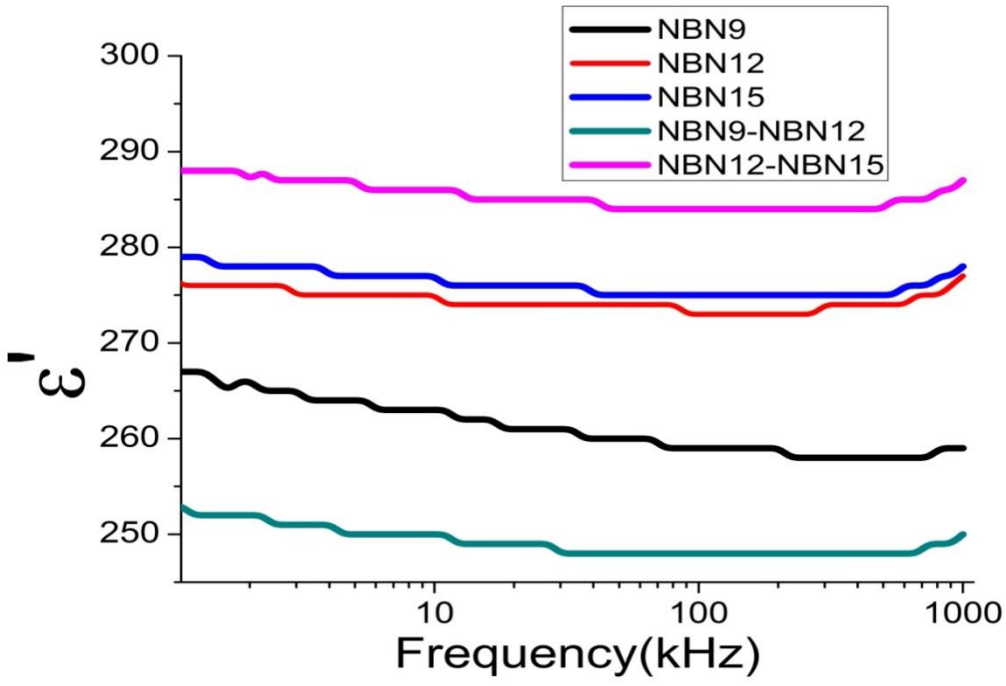

Fig. 15 Permittivity Vs. Frequency plot

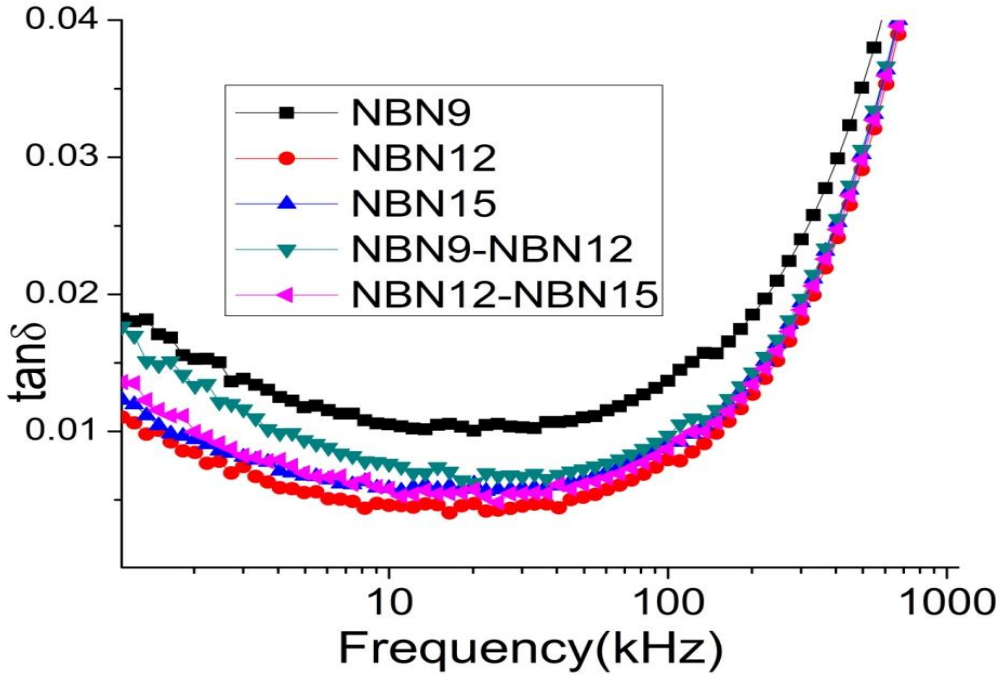

Fig.-16 *tanδ* Vs frequency plot

Figure-17 shows the Polarisation-Electric field loop for different compounds. As expected higher is the no. of perovskite layer higher is the P_r and E_c . The intergrowth also shows similar behaviour.

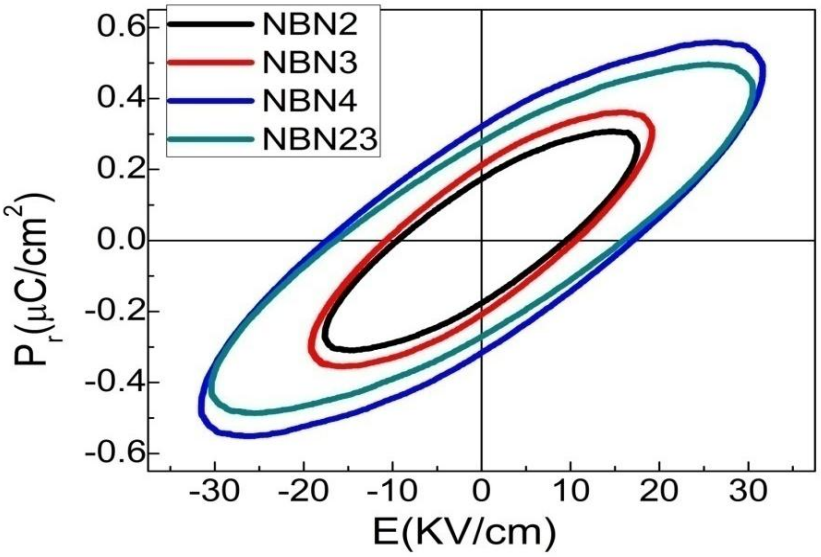

Fig.-17 Polarization Vs Electric field plot

Conclusion

2-layer, 3-layer & 4-layer pure BLSF compounds $Bi_{2.5}Na_{0.5}Nb_20_{9,}$ $Bi_{2.5}Na_{1.5}Nb_30_{12}$& $Bi_{2.5}Na_{2.5}Nb_40_{15}$ and 2-3 and 3-4 layer intergrowth compounds $Bi_{2.5}Na_{0.5}Nb_20_9$-$Bi_{2.5}Na_{1.5}Nb_30_{12}$, $Bi_{2.5}Na_{1.5}Nb_30_{12}$-$Bi_{2.5}Na_{2.5}Nb_40_{15}$ were successfully synthesised through solid oxide reaction route. Phase pure compounds powder were synthesised by calcining the precursor powder at a temperature as low as 800^{o}C. The compounds were sintered to more than 90% of their theoretical density at a temperature of 1100^{o}C. The ceramics shows typical plate like grains due to their very long *c* axis dimension. The 3-4 intergrowth compound shows the highest permittivity and a low *tanδ* indicating that the dielectric properties are enhanced by intergrowth formation.

References

[1] B. Aurivillius, Ark. Kemi 1 (1949) 463.

[2] C.A.P.de Araujo, J.D. Cuchiaro, L.D. McMillan, M. Scott, J.F. Scott,Nature 374 (1995) 627.

[3] B.H. Park, B.S. Kang, S.D. Bu, T.W. Noh, J. Lee, W. Joe, Nature 401 (1999) 682.

[4] S. Obregon Alfaro, A. Martinez-de la Cruz, Applied Catalysis A: General 383 (2010) 128.

[5] H. Yan, H. Zang, M.J. Reece, X. Dong, Appl. Phys. Lett. 87 (2005) 082911.

[6] F. Chu, D. Damjanovic, O. Steiner, N. Setter, J. Am. Ceram. Soc. 78 (1995) 3142.

[7] H.S. Shulman, M. Testorf, D. Damjanovic, N. Setter, J. Am. Ceram. Soc. 79 (1996) 3124.

[8] J.A. Horn, S.C. Zhang, U. Selvaraj, G.L. Messing, S. Trolier-McKinstry, J. Am. Ceram. Soc. 82 (1999) 921.

[9] S.K. Rout, E. Sinha, A. Hussain, J.S. Lee, C.W. Ahn, I.W. Kim, S.I. Woo, J. Appl. Phys. 105 (2009) 024105.

[10] S.H. Hong, S. Trolier-McKinstry, G. L. Messing, J. Am. Ceram. Soc. 83 (2000) 113.

[11] P. Goel, K.L. Yadav, Physica B 382 (2006) 245.

[12] R. Mazumder, A. Sen, H.S. Maiti, Mater. Lett. 58 (2004) 3201.

[13] J. Tellier, P. Boullay, D. B. Jennet, D. Mercurio, Solid State Sciences 10 (2008) 177.

[14] E.C. Subbarao, J. Phys. Chem. Solids 23 (1962) 665.

[15] H.C. Gupta, Archana, V. Luthra, J. Mol. Struct. 984 (2010) 204.

[16] M. Tripathy, R. Mani, J. Gopalakrishnan, Mater. Res. Bull. 42 (2007) 950.

[17] J. Tellier, Ph. Boullay, M. Manier, D. Mercurio, J. Solid State Chem.177 (2004) 1829.

[18] R.E. Newnham, R.W. Wolfe, J.F. Dorrian, Mater. Res. Bull. 6 (1971) 1029.

[19] A.D. Rae, J.G. Thompson, R.L.Withers, Acta Crystallogr. Sect. B: Struct. Sci. 48 (1992) 418.

[20] S.K. Kim, M. Miyama, H. Yanagida, Mater. Res. Bull. 31 (1996) 121.

[21] M. Stachiotti, C. Rodriguez, C.A. Draxl, N. Christensen, Phys. Rev. B 61 (2000) 14434.

[22] T. Kikuchi, Mater. Res. Bull. 14, 1561 (1979).

[23] Stefan Borg,G.oran Svensson,and Jan-Olov Bovin, Journal of Solid State Chemistry 167, 86–96 (2002).

[24] KikuchiT, *Jou. of less-common metals*, 52 (1977) 163-165.

[25] KikuchiT, WatanabeA & Uchida K, *Mater. Res. Bull.*, 12 (1977) 299-304.

[26] Wang X, US007872403B2.

[27] Furukawa M, Tanaka D,Takenaka T, Nagata H &Hiruma Y, US20110241483A1.

[28] Noguchi Y, Miyayama&Kudo T, *Appl. Phys. Lett*., 77 (2000) 3639.

[29] Wang W, Zhu J, Mao X & Chen X,*Mater. Res. Bull*., 42 (2007) 274-280.

[30] Kawada S, OgawaH, KimuraM, ShiratsuyuK & HiguchiY,*J. Appl. Phys*., 46 (2007) 7079.

[31] Ogawa H, Kawada S, Kimura M, Shiratsuyu K &Sakabe Y, *IEEE Trans. Ultrason. Ferroelectr. Freq. control*, 54 (2007) 2500.